Semantic-ICP: Iterative Closest Point for Non-rigid Multi-Organ Point Cloud Registration

Wanwen Chen[1], Carson Studders[2], Jamie J.Y. Kwon[3], Emily H.T. Pang[4], Eitan Prisman[3], and Septimiu E. Salcudean[1]

[1] Department of Electrical and Computer Engineering, University of British Columbia, Canada
{wanwenc,tims}@ece.ubc.ca
[2] Faculty of Medicine, University of British Columbia, Canada
[3] Division of Otolaryngology-Head & Neck Surgery, Department of Surgery, University of British Columbia, Canada
[4] Department of Radiology, University of British Columbia, Canada

Abstract. Point cloud registration is important in computer-aided interventions (CAI). While learning-based point cloud registration methods have been developed, their clinical application is hampered by issues of generalizability and explainability. Therefore, classical point cloud registration methods, such as Iterative Closest Point (ICP), are still widely applied in CAI. ICP methods fail to consider that: (1) the points have well-defined semantic meaning, in that each point can be related to a specific anatomical label; (2) the deformation needs to follow biomechanical energy constraints.

In this paper, we present a novel semantic ICP (sem-ICP) method that handles multiple point labels and uses linear elastic energy regularization. We use semantic labels to improve the robustness of the closest point matching and propose a new point cloud deformation representation to apply explicit biomechanical energy regularization. Our experiments on the Learn2reg abdominal MR-CT registration dataset and a trans-oral robotic surgery ultrasound-CT registration dataset show that our method improves the Hausdorff distance compared with other state-of-the-art ICP-based registration methods. We also perform a sensitivity study to show that our rigid initialization achieves better convergence with different initializations and visible ratios. Sem-ICP code will accompany the published paper.

Keywords: Point cloud registration · Iterative Closest Point · Elastic Energy Regularization.

1   Introduction

Image registration is an important problem in computer-aided intervention (CAI). To enhance visualization of preoperative surgical planning, CAI systems require registration of preoperative volumes to intraoperative volumes, meshes, or surfaces. Compared to dense volumes, point clouds describe critical anatomical
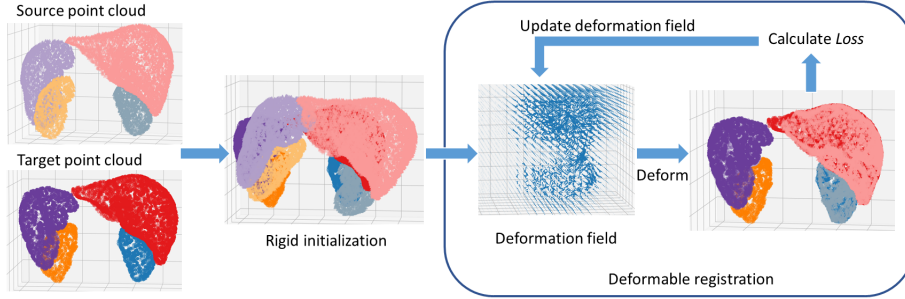
structures as spatial points and provide a modality-agnostic, sparse and flexible representation of meshes and surfaces. Although learning-based point cloud registration methods achieve higher accuracy, they are data-hungry and struggle to generalize to different tasks. Classical point cloud registration methods, therefore, are still widely used in CAI systems where training data are limited and explainability is required. In augmented reality (AR) surgery guidance systems, Iterative Closest Point (ICP) [3] is popular [16] and has been applied in recent navigation systems for spine surgery [14], oral and maxillofacial surgery [2] and neural surgery [15]. ICP is sensitive to initialization and outliers and tends to get trapped in local minima. To solve these problems, Global-ICP [22] searches the entire 3D space to reach global optimality. Fast-robust-ICP [27] uses Welsch's function to improve the robustness of the error metric. However, these methods estimate a rigid transformation, which cannot correct the surface deformation and thus limits their utility. Non-rigid ICP [1] has been used in ultrasound (US)-guided AR navigation for liver procedures [17]. More recent non-rigid ICP registration methods focus on accelerating convergence and improving robustness. Yao et al. [23] use a deformation graph with a globally smooth robust estimator to regularize the deformation, and then use accelerated optimization to improve the runtime [24]. These methods [23,24] have shown improved accuracy compared with non-rigid ICP [1], but they do not consider the medical semantic information and biomechanics energy constraints.

ICP methods [3,1] were originally designed for general computer vision; they can be improved by utilizing specific medical domain knowledge. First, the semantic information of the point cloud, such as the points' anatomical labels, can lead to more robust point matching. Indeed, the images to be matched can be segmented using a variety of methods, including modern deep learning, or novel imaging modalities, such as the ultrasound T-mode™, that can identify tissue type automatically [20]. The workflow of using segmentation for registration is common in 3D volume registration [19,26], and has been explored in point cloud registration. Zaganidis et al. [25] and Wang et al. [21] use the point labels to match the points with similar semantic meanings for lidar point clouds. However, they use rigid registration, which cannot correct for surface deformation. Jiang et al. [11] use point cloud segmentation to perform initial alignment for US-CT registration of the ribs. While they do employ non-rigid point cloud refinement, the refinement relies on the specific graph structure of cartilages. A generalizable non-rigid registration method that does not rely on specific anatomical structures can have a broader application. Second, non-rigid ICP-based registration [1,23,24] regularizes the deformation field by local affine regularization to encourage smoother deformation, but it does not optimize the biomechanical energy. They represent the deformation field as surface point movement that only describes the boundary conditions of the deformation field, making biomechanical modeling challenging. Biomechanics regularization has not been introduced to ICP, and is only implicitly introduced through learning from finite element simulation [8,9]. A novel explicit biomechanics energy regularization is needed for medical point cloud registration.

In this paper, we propose a new method for medical point cloud registration considering the aspects above. Our method extends ICP to provide a more stable initial rigid registration and non-rigid refinement. Our contributions include: (1) using semantic labels in non-rigid ICP to improve the method's accuracy; (2) proposing a novel deformation representation in point clouds; and (3) introducing explicit biomechanical energy regularization into point cloud registration. To the best of our knowledge, this is the first work to use semantic labels for non-rigid point cloud alignment and the first work to use explicit biomechanical energy regularization in point cloud registration. We tested our method on two entirely different datasets to show that it can be generalized to different tasks.

2 Methods

Our method registers the source point cloud $P = \{\boldsymbol{p_0}, \boldsymbol{p_1}, ..., \boldsymbol{p_N}\}$ to the target point cloud $Q = \{\boldsymbol{q_0}, \boldsymbol{q_1}, ..., \boldsymbol{q_M}\}$. The point clouds are associated with semantic labels $L_p = \{x_0, x_1, ..., x_N\}$ and $L_q = \{y_0, y_1, ..., y_N\}$, where the labels belong to the label set $L = \{l_0, l_1..., l_K\}$. We assume that the observed points have at least two labels. Points are associated with local normals $N_p = \{\boldsymbol{n_0}, ..., \boldsymbol{n_N}\}$, $N_q = \{\boldsymbol{m_0}, ..., \boldsymbol{m_M}\}$, which can be estimated using ball pivoting to reconstruct the surfaces. The registration workflow is shown in Fig. 1. We first estimate a rigid registration $\boldsymbol{T} \in SE(3)$, then a non-rigid registration. Instead of parameterizing the deformation as the movement at each point, we uniformly sample C control points $\boldsymbol{r}$ in the point cloud bounding box to describe the deformation field D, and we use trilinear interpolation to estimate the deformation $\boldsymbol{d}$ at point $\boldsymbol{p}$.

Fig. 1. The workflow of our proposed Sem-ICP. The method includes a rigid initialization, then the deformation is estimated iteratively.

Rigid initialization. The rigid registration is iteratively estimated to maximize point cloud similarity. We use the semantic information during point pair matching, so matched point pairs have the same semantic labels. At each iteration i, for each label $l \in L$, we perform closest point matching in a subset of the point

clouds P_{sub} and Q_{sub}, where the points have the same label l. We use KD-trees for a quick search of point pairs $(\boldsymbol{p}_j^i, \boldsymbol{q}_j^i)$. Instead of using point-to-point distance as in ICP, we use the point-to-plane loss in Eq. 1 to encourage the matched point pairs to be on the same plane. We use the Adam optimizer [12] to find the rigid transformation $\boldsymbol{R}, \boldsymbol{t}$, with $\boldsymbol{R}$ parametrized by XYZ Euler angles, that minimizes the loss:

$$L_{rigid}(\boldsymbol{R}, \boldsymbol{t}) = \sum_{j=1}^{N} |(\boldsymbol{R}\boldsymbol{p}_j^i + \boldsymbol{t} - \boldsymbol{q}_j^i) \cdot \boldsymbol{m_j}| \tag{1}$$

The iteration is repeated until the loss is no longer improved or the method reaches the maximum number of iterations.

Non-rigid registration. Non-rigid registration is performed after the initial rigid alignment. We use trilinear interpolation to estimate the surface point deformation $\boldsymbol{d}$ at point $\boldsymbol{p}$. In each iteration i, we use the same label-informed nearest point matching method employed earlier during rigid initialization to find the matched point pair $(\boldsymbol{p}_j^i, \boldsymbol{q}_j^i)$, and use the Adam optimizer to minimize the loss in Eq. 2. The first term minimizes the distance between the matched point pairs, while the remaining regularization terms control tissue deformation.

$$L_{non-rigid}(D) = \sum_{j=1}^{N} ||\boldsymbol{p}_j^i + \boldsymbol{d}_j^i - \boldsymbol{q}_j^i||_2 + Reg_{els}(D) + Reg_{mag}(D) + Reg_{grad}(D) \tag{2}$$

Our new point cloud deformation field representation provides several improvements over the state of the art. The control point-based representation is more consistent in memory usage since it does not depend on the density of the input point clouds. Individual point movement is more regularized because it is interpolated from neighboring control points. More importantly, this new deformation representation enables *explicit* biomechanics-based regularization, since it also models the inner tissue deformation rather than only describing the boundary conditions. We use linear elastic regularization [7,18] to achieve a deformation field with optimal elastic energy. In continuum mechanics, the linear elastic energy can be described using the Navier-Lamé Equation (Eq. 3):

$$Reg_{els}(D) = \int_{Vol} \left(\frac{\mu}{4} \sum_{j=1}^{3} \sum_{k=1}^{3} \left(\frac{\partial D_j}{\partial x_k} + \frac{\partial D_k}{\partial x_j}\right) + \frac{\lambda}{2}(\nabla D)^2\right) dx \tag{3}$$

where λ and μ are Lamé parameters. These parameters can be estimated based on Young's modulus E and Poisson's ratio ν:

$$\lambda = \frac{E\nu}{(1+\nu)(1-2\nu)} \ , \ \mu = \frac{E}{2(1+\nu)} \tag{4}$$

In the absence of tissue biomechanical labels, we assume that all the tissues have a Young's modulus of $E = 1\text{kPa}$ [4] and are almost incompressible, with a Poisson's ratio of $\nu = 0.499$. Multiple E and ν can be employed if tissue

labels include this information, e.g., from elastography. The uniformly sampled deformation field allows us to implement a discrete approximation of Eq. 3.
In addition to the above energy regularization, we use a magnitude regularization in Eq. 2 to reduce unwanted large deformation, and a gradient regularization to encourage control grid smoothness:

$$Reg_{mag}(D) = \frac{1}{C} \sum_i^C ||\boldsymbol{r_i}||_2 \,;\ Reg_{grad}(D) = \frac{1}{C} \sum_{x,y,z}^C ||\frac{\partial D}{\partial x}||_2 + ||\frac{\partial D}{\partial y}||_2 + ||\frac{\partial D}{\partial z}||_2$$

3 Experiments

Datasets. We evaluated our method on two datasets.
AbdominalMRCT: The paired point clouds are from the Learn2reg intra-patient abdominal magnetic resonance (MR)-computerized tomography (CT) registration challenge [5,10], which is shared under Creative Commons Attribution 3.0 Unported License. We use the training data since label maps for test data are not included in the open dataset. We use only the data with paired MR and CT. The resulting curated dataset has 8 pairs of intra-patient MR and CT, and the provided label maps include 3D segmentation of the liver, spleen, and left and right kidneys. We extracted the meshes of the labels using 3D Slicer [6].
TORS: This is a private dataset containing neck 3D freehand ultrasound (US) and CT images collected from patients who underwent transoral robotic surgery (TORS) for oral cancer from January 2022 to October 2023 at Vancouver General Hospital (Vancouver, BC, Canada). This study received ethics approval from the University of British Columbia Clinical Research Ethics Board (H19-04025). The diagnostic CT data were collected preoperatively, and the US data were collected before surgery while patients were under anesthesia. A BK3500 with a 14L3 linear 2D transducer (BK Medical, Burlington, MA) and a Polaris Spectra (Northern Digital, ON, Canada) were used to collect freehand 3D US. We used PLUS [13] to perform US probe calibration, collect tracked US data, and perform 3D reconstruction. The image depth was set to 4 or 5 cm (depending on patient anatomy) at 9 MHz, and US imaging was done ipsilateral to the tumor. A medical student and an experienced research assistant labeled the carotid artery, jugular vein, and larynx in 2D US frames and CT volumes, then the 2D US label maps were reconstructed to 3D. The dataset contains 18 pairs of US-CT images from 7 patients. The volumes were resampled to an isotropic resolution of 0.8mm and prealigned based on the center and the axis of the carotid. 3D Slicer was used to convert the 3D label maps to meshes.

Selected baselines. We compare our method with established rigid and non-rigid ICP-based point cloud registration methods. For rigid registration, the baseline methods are the original ICP [3] and its recent variants Global-ICP (GO-ICP) [22] and Fast-robust-ICP (FastICP) [27]. For non-rigid registration, we compare with NR-ICP [1], Fast-NRR [23] and AMM-NRR [24]. We used the default parameters of the baselines provided in their open-source codes.

Implementation Details. The methods were implemented with a 12GB Nvidia GeForce RTX 3060 GPU, using Python 3.9.18, PyTorch 2.1.2, and CUDA-11.8. We used an Adam optimizer with a learning rate of 0.1. The maximum number of iterations is 500 for rigid initialization and 300 for non-rigid refinement, and the optimization is ended when the loss is no longer improved. Each coordinate of the points was normalized to [0,1] for better convergence, and we uniformly sampled $20 \times 20 \times 20$ control points in the $[0, 1]^3$ space.
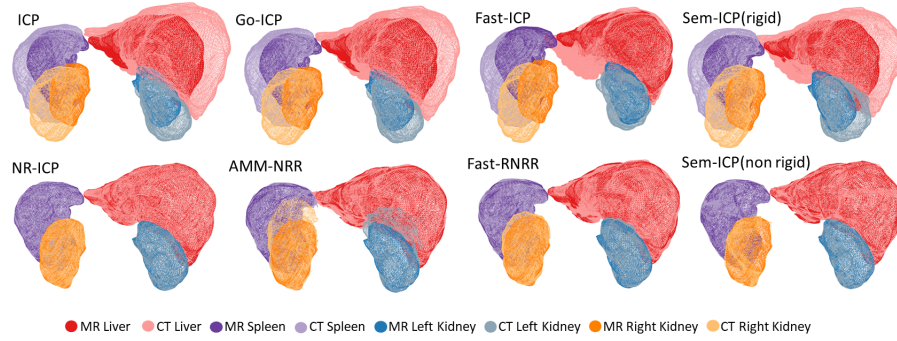
4   Results and Discussion

Evaluation on datasets. The Hausdorff distances (HD) for registration on AbdominalMRCT dataset are shown in Table 1, and the qualitative results are shown in Fig. 2. Our method achieves the lowest HD for all organs compared to other baselines. The challenge of this dataset is that the organs undergo significant deformation, so all rigid registration methods have a relatively large HD. Non-rigid registration is essential to estimate the deformation. Fig. 2 demonstrates that non-rigid registration algorithms can mismatch points from different organs, especially for AMM-NRR and Fast-RNRR, while our method maintains a clear boundary. Similar results are observed with the TORS dataset, as shown in Table 2 and Fig. 3. One unique challenge associated with this dataset is that the US volumes provide only partial observation of the anatomical structures, especially of the larynx. Our results show that other non-rigid registration methods have larger HD when registering all anatomical structures, especially in the larynx HD. Without semantic information, other non-rigid registration algorithms under-penalize the larynx registration error, which increases the class-specific registration error. These results show that our method improves the delineation of anatomical structures and leads to significantly lower HD across all organ point clouds, greatly improving registration accuracy. Our novel deformation registration algorithm provides a simple and effective way to model biomechanical energy in point cloud registration. NR-ICP, AMM-NRR and Fast-RNRR regularize the deformation with a local affine regularization, which can over-smooth the deformation, increasing the registration errors. Our biomechanical energy-based regularization is inspired by physics, which can generate more realistic and accurate alignment.
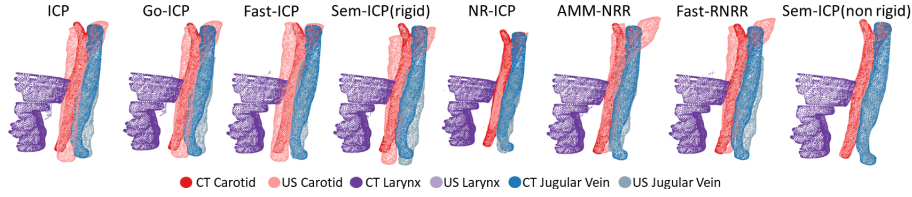
Sensitivity study. To assess the sensitivity of our method and its robustness with respect to initial poses, we simulated partial observations and applied different rigid misalignments to the Learn2reg MR point clouds. We simulated point clouds with 10%, 20%, 50% and 80% of points visible, and introduced additional Gaussian noise. Ten different simulated partial point clouds with random rigid transformation were generated for each patient, resulting in a total of 80 simulations. Table 3 shows that our rigid initialization achieves lower HD and target registration error (TRE) compared to the other rigid ICP baselines. These results demonstrate that using semantic labels in point cloud registration improves the rigid registration step accuracy in different initialization positions. This first stage of registration is further improved with non-rigid refinement.

Table 1. The average Hausdorff distances on the Learn2reg AbdominalMRCT. The metrics are reported in mean (std) in *mm*.

Label	ICP	GO-ICP	FastICP	SemICP (rigid)	NR-ICP	AMM-NRR	Fast-RNRR	SemICP (refine)
Liver	29.08 (8.15)	28.28 (7.41)	37.23 (15.12)	30.90 (9.07)	14.04 (4.35)	22.92 (7.59)	23.45 (17.54)	**10.01** **(4.82)**
Spleen	23.17 (6.54)	22.88 (6.78)	26.49 (11.00)	24.01 (7.85)	9.24 (5.66)	15.14 (5.16)	15.51 (12.73)	**7.12** **(4.34)**
KidneyL	19.96 (7.83)	19.88 (7.51)	20.98 (8.51)	19.32 (7.77)	9.06 (4.70)	28.85 (27.31)	23.21 (19.90)	**8.93** **(3.86)**
KidneyR	27.29 (9.86)	27.77 (9.74)	28.30 (10.38)	25.49 (10.01)	12.14 (4.53)	31.02 (19.64)	24.42 (15.90)	**9.15** **(2.97)**

● MR Liver ● CT Liver ● MR Spleen ● CT Spleen ● MR Left Kidney ● CT Left Kidney ● MR Right Kidney ● CT Right Kidney

Fig. 2. Qualitative results on AbdominalMRCT dataset.

Table 2. The average Hausdorff distances on the TORS dataset. The metrics are reported in mean (std) in *mm*.

Label	ICP	GO-ICP	FastICP	SemICP (rigid)	NR-ICP	AMM-NRR	Fast-RNRR	SemICP (refine)
Carotid	9.18 (2.92)	8.09 (3.10)	9.37 (3.04)	7.62 (2.47)	6.27 (3.02)	7.72 (3.39)	7.96 (2.76)	**2.96** **(0.53)**
Larynx	8.16 (4.69)	8.77 (6.03)	8.55 (5.23)	8.67 (3.61)	9.74 (8.86)	11.40 (8.19)	15.17 (5.87)	**1.19** **(0.57)**
Vein	8.46 (5.15)	7.71 (5.00)	8.00 (5.16)	6.39 (2.09)	5.50 (2.62)	7.34 (2.88)	8.19 (2.99)	**2.36** **(2.05)**

Fig. 3. Qualitative results on TORS dataset.

Table 3. The average Hausdorff distance (HD) of all labels and target registration error (TRE) for different rigid ICP methods with variant visible ratios of the point cloud. The numbers are reported in *mm*.

	ICP		GO-ICP		FastICP		SemICP(rigid)		SemICP(refine)	
Vis-ratio	HD	TRE	HD	TRE	HD	TRE	HD	TRE	HD	TRE
10%	115.97	143.19	91.78	87.15	114.46	122.91	58.7	54.76	**11.26**	**35.45**
20%	126.87	127.03	128.36	121.98	121.72	123.63	60.09	47.04	**12.36**	**32.60**
50%	142.82	132.64	136.92	119.67	125.95	119.65	73.22	45.57	**15.2**	**30.89**
80%	136.13	136.02	137.37	122.02	119.73	113.97	80.04	45.77	**16.6**	**31.52**

Limitations and future work: Our work requires semantic labels in the point cloud, and this paper focuses on registration without discussing the point cloud labeling process. Labels from preoperative images are often generated manually, but intraoperative labeling can hinder real-time applications. In future work, we plan to investigate deep-learning models to perform intraoperative segmentation for the full registration pipeline. Additionally, this method is designed for multi-organ registration, but it has the potential to be generalized to single-organ registration as long as the point clouds have different semantic labels (such as using vessels inside the liver as additional labels). Finally, the homogeneous linear elastic energy is a simplified model, and we plan to explore the use of different biomechanical parameters for different control points based on the type of tissue and its properties.

5   Conclusion

We present a novel non-rigid registration method that introduces semantic label-based point matching into ICP to improve the quality of the matched point pairs. Additionally, this new method utilizes a novel control point-based deformation representation to enable explicit biomechanics-based regularization in point cloud registration. Our method outperforms state-of-the-art point matching-based registration methods on two different datasets, showing that it is generalizable to different tasks.

Disclosure of Interests. The authors have no competing interests to declare that are relevant to the content of this article.

References

1. Amberg, B., Romdhani, S., Vetter, T.: Optimal step nonrigid icp algorithms for surface registration. In: 2007 IEEE conference on computer vision and pattern recognition. pp. 1–8. IEEE (2007)
2. Bayrak, M., Alsadoon, A., Prasad, P., Venkata, H.S., Ali, R.S., Haddad, S.: A novel rotation invariant and manhattan metric–based pose refinement: Augmented reality–based oral and maxillofacial surgery. The International Journal of Medical Robotics and Computer Assisted Surgery **16**(3), e2077 (2020)
3. Besl, P.J., McKay, N.D.: Method for registration of 3-d shapes. In: Sensor fusion IV: control paradigms and data structures. vol. 1611, pp. 586–606. Spie (1992)
4. Chen, E., Novakofski, J., Jenkins, W., O'Brien, W.: Young's modulus measurements of soft tissues with application to elasticity imaging. IEEE Transactions on Ultrasonics, Ferroelectrics, and Frequency Control **43**(1), 191–194 (1996). https://doi.org/10.1109/58.484478
5. Clark, K., Vendt, B., Smith, K., Freymann, J., Kirby, J., Koppel, P., Moore, S., Phillips, S., Maffitt, D., Pringle, M., et al.: The cancer imaging archive (tcia): maintaining and operating a public information repository. Journal of digital imaging **26**, 1045–1057 (2013)
6. Fedorov, A., Beichel, R., Kalpathy-Cramer, J., Finet, J., Fillion-Robin, J.C., Pujol, S., Bauer, C., Jennings, D., Fennessy, F., Sonka, M., et al.: 3d slicer as an image computing platform for the quantitative imaging network. Magnetic resonance imaging **30**(9), 1323–1341 (2012)
7. Fischer, B., Modersitzki, J.: A unified approach to fast image registration and a new curvature based registration technique. Linear Algebra and its applications **380**, 107–124 (2004)
8. Fu, Y., Lei, Y., Wang, T., Patel, P., Jani, A.B., Mao, H., Curran, W.J., Liu, T., Yang, X.: Biomechanically constrained non-rigid mr-trus prostate registration using deep learning based 3d point cloud matching. Medical image analysis **67**, 101845 (2021)
9. Fu, Y., Wang, T., Lei, Y., Patel, P., Jani, A.B., Curran, W.J., Liu, T., Yang, X.: Deformable mr-cbct prostate registration using biomechanically constrained deep learning networks. Medical physics **48**(1), 253–263 (2021)
10. Hering, A., Hansen, L., Mok, T.C., Chung, A.C., Siebert, H., Häger, S., Lange, A., Kuckertz, S., Heldmann, S., Shao, W., et al.: Learn2reg: comprehensive multi-task medical image registration challenge, dataset and evaluation in the era of deep learning. IEEE Transactions on Medical Imaging **42**(3), 697–712 (2022)
11. Jiang, Z., Kang, Y., Bi, Y., Li, X., Li, C., Navab, N.: Class-aware cartilage segmentation for autonomous us-ct registration in robotic intercostal ultrasound imaging. IEEE Transactions on Automation Science and Engineering pp. 1–13 (2024). https://doi.org/10.1109/TASE.2024.3411784
12. Kinga, D., Adam, J.B., et al.: A method for stochastic optimization. In: International conference on learning representations (ICLR). vol. 5, p. 6. San Diego, California; (2015)

13. Lasso, A., Heffter, T., Rankin, A., Pinter, C., Ungi, T., Fichtinger, G.: Plus: open-source toolkit for ultrasound-guided intervention systems. IEEE transactions on biomedical engineering **61**(10), 2527–2537 (2014)
14. Liebmann, F., von Atzigen, M., Stütz, D., Wolf, J., Zingg, L., Suter, D., Cavalcanti, N.A., Leoty, L., Esfandiari, H., Snedeker, J.G., et al.: Automatic registration with continuous pose updates for marker-less surgical navigation in spine surgery. Medical Image Analysis **91**, 103027 (2024)
15. Liu, Z., Yang, Z., Jiang, S., Zhou, Z.: A spatial registration method based on point cloud and deep learning for augmented reality neurosurgical navigation. The International Journal of Medical Robotics and Computer Assisted Surgery **20**(6), e70030 (2024)
16. Ma, L., Huang, T., Wang, J., Liao, H.: Visualization, registration and tracking techniques for augmented reality guided surgery: a review. Physics in Medicine & Biology **68**(4), 04TR02 (2023)
17. Ma, L., Liang, H., Han, B., Yang, S., Zhang, X., Liao, H.: Augmented reality navigation with ultrasound-assisted point cloud registration for percutaneous ablation of liver tumors. International journal of computer assisted radiology and surgery **17**(9), 1543–1552 (2022)
18. Nir, G., Sahebjavaher, R.S., Kozlowski, P., Chang, S.D., Sinkus, R., Goldenberg, S.L., Salcudean, S.E.: Model-based registration of ex vivo and in vivo mri of the prostate using elastography. IEEE transactions on medical imaging **32**(6), 1068–1080 (2013)
19. Siebert, H., Hansen, L., Heinrich, M.P.: Fast 3d registration with accurate optimisation and little learning for learn2reg 2021. In: International Conference on Medical Image Computing and Computer-Assisted Intervention. pp. 174–179. Springer (2021)
20. Stephens, K.: Clarius launches t-mode ai for ultrasound. AXIS Imaging News (2024)
21. Wang, Q., Yang, Y., Wan, T., Du, S.: Robust point set registration based on semantic information. In: 2020 IEEE International Conference on Systems, Man, and Cybernetics (SMC). pp. 2553–2558. IEEE (2020)
22. Yang, J., Li, H., Campbell, D., Jia, Y.: Go-icp: A globally optimal solution to 3d icp point-set registration. IEEE transactions on pattern analysis and machine intelligence **38**(11), 2241–2254 (2015)
23. Yao, Y., Deng, B., Xu, W., Zhang, J.: Quasi-newton solver for robust non-rigid registration. In: Proceedings of the IEEE/CVF conference on computer vision and pattern recognition. pp. 7600–7609 (2020)
24. Yao, Y., Deng, B., Xu, W., Zhang, J.: Fast and robust non-rigid registration using accelerated majorization-minimization. IEEE Transactions on Pattern Analysis and Machine Intelligence **45**(8), 9681–9698 (2023)
25. Zaganidis, A., Sun, L., Duckett, T., Cielniak, G.: Integrating deep semantic segmentation into 3-d point cloud registration. IEEE Robotics and automation letters **3**(4), 2942–2949 (2018)
26. Zeng, Q., Mohammed, S., Pang, E.H., Schneider, C., Honarvar, M., Lobo, J., Hu, C., Jago, J., Ng, G., Rohling, R., et al.: Learning-based us-mr liver image registration with spatial priors. In: International conference on medical image computing and computer-assisted intervention. pp. 174–184. Springer (2022)
27. Zhang, J., Yao, Y., Deng, B.: Fast and robust iterative closest point. IEEE Transactions on Pattern Analysis and Machine Intelligence **44**(7), 3450–3466 (2022)